AD_____

Award Number: DAMD17-03-1-0752

TITLE: Development of Quantum Dot Probes for Near-Infrared Fluorescence Imaging of Breast Cancer Angiogenesis

PRINCIPAL INVESTIGATOR: Xiaoyuan Chen, Ph.D.

CONTRACTING ORGANIZATION: University of Southern California
Los Angeles, California 90089-9074

REPORT DATE: September 2004

TYPE OF REPORT: Final

PREPARED FOR: U.S. Army Medical Research and Materiel Command
Fort Detrick, Maryland 21702-5012

DISTRIBUTION STATEMENT: Approved for Public Release;
Distribution Unlimited

The views, opinions and/or findings contained in this report are those of the author(s) and should not be construed as an official Department of the Army position, policy or decision unless so designated by other documentation.

20050505 076

REPORT DOCUMENTATION PAGE

Form Approved
OMB No. 074-0188

Public reporting burden for this collection of information is estimated to average 1 hour per response, including the time for reviewing instructions, searching existing data sources, gathering and maintaining the data needed, and completing and reviewing this collection of information. Send comments regarding this burden estimate or any other aspect of this collection of information, including suggestions for reducing this burden to Washington Headquarters Services, Directorate for Information Operations and Reports, 1215 Jefferson Davis Highway, Suite 1204, Arlington, VA 22202-4302, and to the Office of Management and Budget, Paperwork Reduction Project (0704-0188), Washington, DC 20503

1. AGENCY USE ONLY (Leave blank)	2. REPORT DATE	3. REPORT TYPE AND DATES COVERED
	September 2004	Final (1 Sep 2003 - 31 Aug 2004)

4. TITLE AND SUBTITLE
Development of Quantum Dot Probes for Near-Infrared Fluorescence Imaging of Breast Cancer Angiogenesis

5. FUNDING NUMBERS
DAMD17-03-1-0752

6. AUTHOR(S)
Xiaoyuan Chen, Ph.D.

7. PERFORMING ORGANIZATION NAME(S) AND ADDRESS(ES)
University of Southern California
Los Angeles, California 90089-9074

E-Mail: shawchen@stanford.edu

8. PERFORMING ORGANIZATION REPORT NUMBER

9. SPONSORING / MONITORING AGENCY NAME(S) AND ADDRESS(ES)
U.S. Army Medical Research and Materiel Command
Fort Detrick, Maryland 21702-5012

10. SPONSORING / MONITORING AGENCY REPORT NUMBER

11. SUPPLEMENTARY NOTES

12a. DISTRIBUTION / AVAILABILITY STATEMENT
Approved for Public Release; Distribution Unlimited

12b. DISTRIBUTION CODE

13. ABSTRACT (Maximum 200 Words)

The **overall objective** of this proposal is to develop cyclic RGD peptide conjugated biocompatible quantum dot nanoparticles for near-infrared fluorescence imaging of breast cancer angiogenesis. The **two hypotheses** to be tested are that: 1) the integrin alpha(v)beta(3) antagonist, when conjugated with semiconductor nanocrystals, will not change the fluorescent properties of the QDs significantly; and 2) the QD-based breast cancer angiogenesis probes are specific enough to recognize the integrin receptor and bright enough for effective detection in preclinical animal models. **Specific Aim 1**: to prepare water-soluble QD-RGD conjugates and characterize the probes *in vitro*. **Specific Aim 2**: to assess the tumor targeting efficacy of QD-RGD in breast cancer model. **Major Findings**: Although biocompatible quantum dots in theory is superior to organic dyes for long-term, multi-target and highly sensitive imaging, however, the current surface coating techniques do not offer enough stability of QDs in biological medium. On the other hand, NIR fluorescent dyes labeled RGD peptides demonstrated highly sensitive and semi-quantitative NIR fluorescence images for tumor detection in preclinical xenograft models. This non-invasive optical imaging approach provides the opportunity for rapid and cost-effective studies before more costly radionuclide-based imaging studies.

14. SUBJECT TERMS	15. NUMBER OF PAGES
NIR fluorescence, Quantum dots, Cy5.5, Integrin, Angiogenesis	23
	16. PRICE CODE

17. SECURITY CLASSIFICATION OF REPORT	18. SECURITY CLASSIFICATION OF THIS PAGE	19. SECURITY CLASSIFICATION OF ABSTRACT	20. LIMITATION OF ABSTRACT
Unclassified	Unclassified	Unclassified	Unlimited

Table of Contents

INTRODUCTION

Angiogenesis, the formation of new capillaries from the pre-existing blood vessels, is a fundamental process involved in breast cancer tumor growth and metastasis [1]. Molecular imaging of tumor angiogenesis will play a key role in the development of anti-angiogenic therapies [2]. The vitronection receptor $\alpha_v\beta_3$ integrin, which is highly expressed on activated endothelial cells and breast cancer tumor cells, is responsible for a wide range of cell-extracellular matrix and cell-cell interactions [3]. Cyclic RGD peptides have been shown to block tumor angiogenesis without affecting pre-existing blood vessels; radiolabeled RGD peptides have also been shown to be able to demonstrate receptor specific tumor uptake [4]. The emerging field of near-infrared fluorescence (NIRF) imaging has awakened a great deal of interest in developing targeted optical contrast probes as an alternative to radioactive imaging methods, employing relatively low cost instrumentation and using non-ionizing radiation. The deep tissue propagation of Near-infrared (NIR) light between 700 and 900 nm offers new opportunities for diagnostic imaging when employing sensitive detection techniques and NIR excitable fluorescent agents that target and report disease and metabolism [5,6]. Nano-sized semiconductor particles, or quantum dots that have high quantum yields, narrow emission bands, high absorbancy, very long effective Stokes shifts, high resistance to photobleaching, and can provide excitation of several different emission colors using a single wavelength biological application, potentially can provide long-term, multi-target, and highly sensitive optical imaging [7]. This proposal is to compare the NIR fluorescence imaging quality of RGD-QD and RGD-Cy5.5 conjugates for subcutaneous tumor delineation. Specific Aim 1: to prepare water-soluble QD-RGD conjugates and characterize the probes *in vitro*; and Specific Aim 2: to assess the tumor targeting efficacy of QD-RGD in breast cancer model.

BODY

Water-soluble quantum dots are available from both QDots, Inc. (http://www.qdots.com) and Evident Technologies, Inc. (http://www.evidenttech.com). The quantum dots from QDots are always modified with biomolecules, such as biotin, streptavidin, primary antibody, or secondary antibody, which do not allow further modification on the surface. On the other hand, biocompatible quantum dots from Evident Technologies, so-called Evitags, have multiple carboxylate or primary amino function groups are suitable for RGD peptide conjugation. We have thus chosen Evitags for our studies. The quantum core material is comprised of InP. Transmission electron microscope (TEM) analysis indicated that the particles look very uniform in size with an average diameter of 7 nm. They also arrange themselves in very nice arrays (**Fig. 1**). The peak emission wavelength of the InP core EviTags was determined to be in the NIR region at 725 nm (**Fig. 2**).

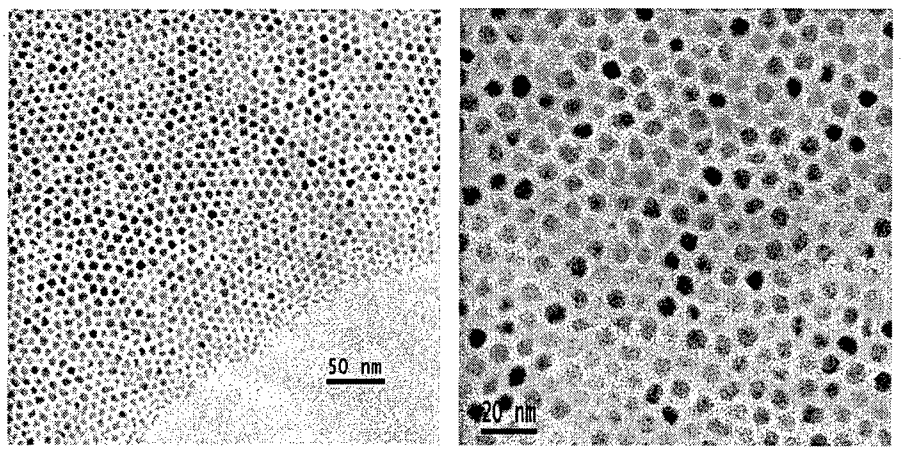

Fig. 1 TEM analysis of NIR emitting InP quantum dot core material. At low magnification (left) the particles are shown to be of relatively uniform size. At higher magnification (right) the average size of the particles can are determined to be approximately 7 nm.

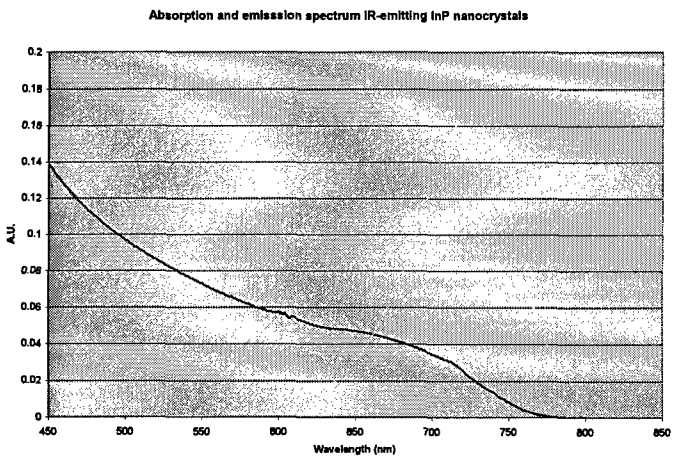

Fig. 2 Absorption and emission spectra of InP. The peak emission wavelength is shown to be at 725 nm.

Conjugation of this carboxylate-Evitag with cyclic RGD peptide is straightforward. The carboxylate groups on the Evitag surface was activated by using EDC and sulfo-NHS to

form sulfonylsuccinimidyl active esters (**Fig. 3**). The unreacted EDC and sulfo-NHS was then removed by spin filtration and coupled with RGD peptides. A schematic structure of the RGD-Evitag conjugate is shown in **Fig. 4**. Monomeric, dimeric and tetrameric RGD peptides (**Fig. 5**) with different integrin receptor bindinga ffinities were tested.

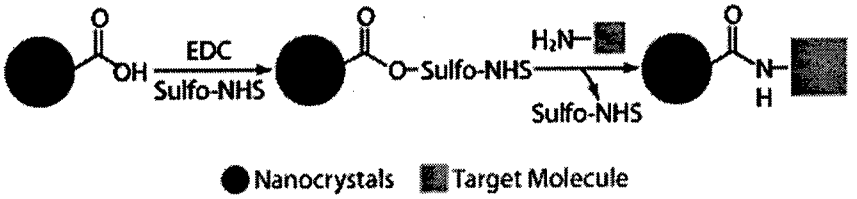

Fig. 3 Covalent immobilization of proteins or peptides to carboxy-EviTags using EDC and sulfo-NHS.

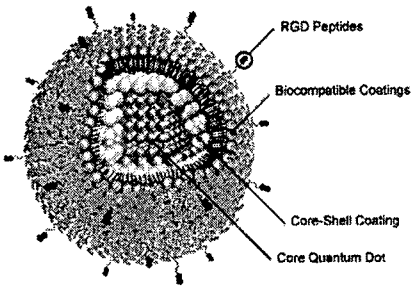

Fig. 4 Schematic illustration of RGD-Evitag conjugate for in vitro and in vivo tumor targeting and imaging. The NIR fluorescence emitting peptide-QD conjugates are expected to have approximately 10 to 35 nanometers in size and 2-20 RGD peptides per nano particle, which may offer advantages of long photostability, unique optical and electronic properties, and polyvalent inetgrin bindings.

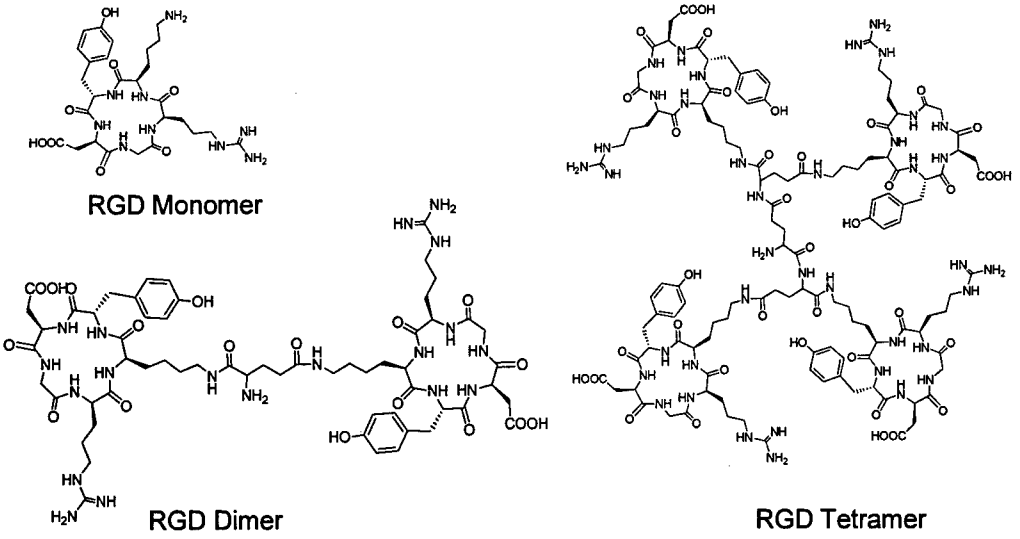

Fig. 5 Structures of monomeric, dimeric and tetrameric RDG peptides. Integrin $\alpha_v\beta_3$ receptor binding affinity of these peptides follows the order of tetramer > dimer > monomer due to polyvalency.

The RGD-conjugated EviTags are highly photo-resistant with fluorescence lifetimes of up to a week under illumination, with little or no photobleaching. We have profiled EviTags against traditional organic fluorophores to illustrate their enhanced photostability (**Fig. 6**). In a dual labeling experiment, nuclear proteins were labeled with FITC and cell surface receptors were labeled with EviTag-antibody conjugates. After 150 seconds of constant exposure to laser excitation, FITC underwent extensive

photobleaching, while the EviTags showed no detectable change in their fluorescence brightness.

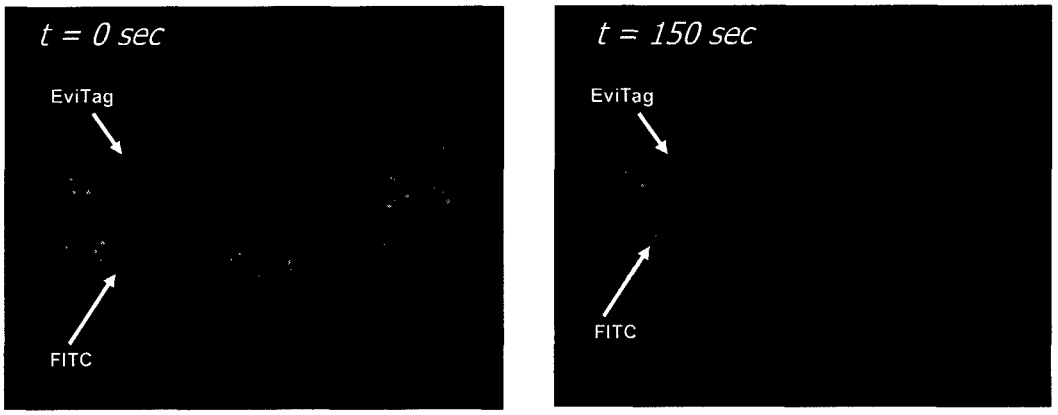

Fig. 6 Fort Orange EviTags (600nm) versus FITC in a double staining of HepG2 cells. At t = 0 sec (left) both the Fort Orange EviTag and FITC fluorophores have similar brightness. After 150 sec of continuous exposure to excitation light, the Fort Orange EviTag brightness is unchanged while the FITC brightness is considerably diminished.

However, when the RGD-Evitag conjugate was injected through tail vein into a nude mouse containing orthotopic MDA-MB-435 tumor xenograft. The quantum dot probe aggregated and clogged in the lung without further distribution. The same phenomenon was observed with Evitags with no RGD peptide modification, presumably due to the lack of suitable surface coating that can maintain high quantum yield and confer stability in biological fluid. In parallel, we tested fluorescent dye labeled RGD peptides for tumor imaging.

We found that different tumor cells express significantly different amount of integrin $\alpha_v\beta_3$. As shown in **Fig. 7**, the $\alpha_v\beta_3$ integrin on breast cancer cell lines (MCF-7, MDA-MB-468, MDA-MB-231, and MDA-MB-435) and brain tumor cells (U87MG) were characterized by Western Blot analysis using monoclonal antibody LM 609. Each cell type displays a different repertoire of $\alpha_v\beta_3$ on the cell surface. All four breast cancer cell lines had significantly lower integrin levels than that of U87MG glioma cell line. Among the breast cancer cells, the integrin levels follow the order of MDA-MB-435 > MDA-MB-231 > MDA-MB-468 > MCF-7, which correlates well with the metastatic potential of these cells and their ability to adhere and migrate as reported in the literature.

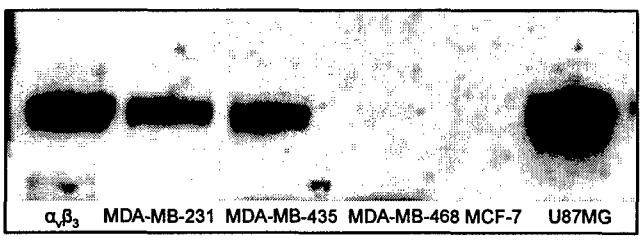

Fig. 7 Western blot analysis for $\alpha_v\beta_3$ integrin in different tumor cells. Lysates were immunoprecipitated with $\alpha_v\beta_3$ specific antibody LM609.

The structure of conjugate coupled between monomeric RGD peptide and Cy5.5 [8]. was shown in **Fig. 8**. The absorption and fluorescence emission characteristics of RGD-Cy5.5 conjugate were similar to those of free Cy5.5, as apparent from the spectra measured in H_2O, except that the emission maximum slightly blue shifted from 694 nm (Cy5.5-NHS ester) to 690 nm (RGD-Cy5.5 conjugate). The yield of RGD-Cy5.5 conjugate was typically 70 to 75% as calculated with $\varepsilon_{678\ nm}$ = 250,000 $(mol/L)^{-1}cm^{-1}$. Modification of the RGD peptide with Cy5.5 somewhat decreased its receptor binding avidity, with the IC_{50} values for c(RGDyK) and RGD-Cy5.5 being 37.5 ± 3.4 nM and 58.1 ± 5.6 nM, respectively.

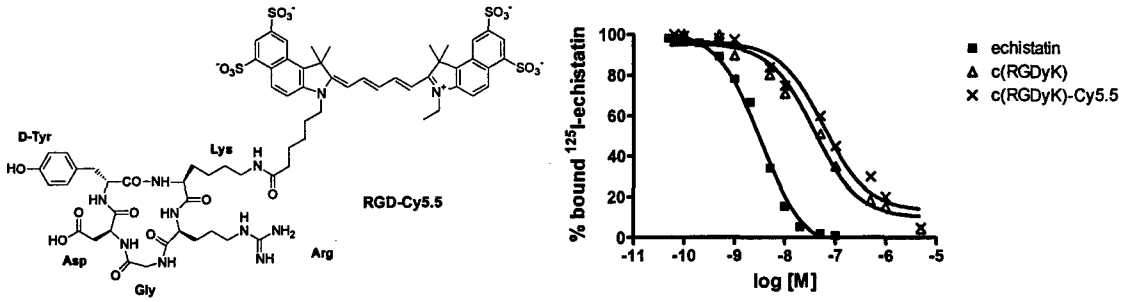

Fig. 8 Left: Schematic structure of the RGD-Cy5.5 conjugate. Right: Competition of specific binding of ^{125}I-echistatin with unlabeled echistatin (■), c(RGDyK) (Δ), and c(RGDyK)-Cy5.5 (×) to purified $\alpha_v\beta_3$ integrin as determined using the solid-phase receptor assay. All points were done in triplicate. Cy5.5 conjugation did not significantly decrease the receptor binding affinity of the resulting fluorescent cyclic RGD peptide.

To demonstrate that the RGD-Cy5.5 conjugate can act as a specific ligand for $\alpha_v\beta_3$ integrin receptor, binding and subcellular localization of cyanine dye labeled RGD peptide were incubated with U87MG tumor cells and HBCEC cells that are known to overexpress $\alpha_v\beta_3$ integrin. Negligible signals were detected in both cell lines when cells were incubated with Cy5.5 dye (data not shown). Receptor mediated endocytosis of the RGD-Cy5.5 conjugate was observed by confocal laser scanning microscopy in both cell types (**Fig. 9**A,C and Fig. 3F, H). Binding of RGD-Cy5.5 to both cells types was completely blocked by co-incubation of the conjugate and c(RGDyK) (1 μM) (**Fig. 9**D, I).

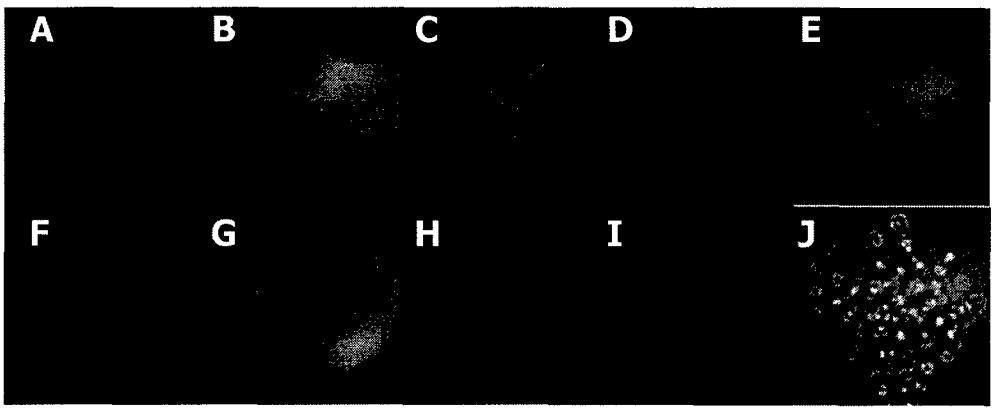

Fig. 9 Specific binding and endocytosis of the Cy5.5 labeled cyclic RGD peptide c(RGDyK). Confocal laser scanning microscopy images of U87MG human glioblastoma (A-E) and HBCEC

human brain capillary endothelial cells (F-J) incubated for 1 h at 37 °C in the presence of 100 nM RGD-Cy5.5 with (D-E, I-J) or without (A-C, F-H) blocking dose of non-fluorescent RGD peptide c(RGDyK) (10 μM). (A, F): NIR fluorescence images of U87MG (A) and HBCEC (F) cells; (B, G): direct visualization of U87MG (B) and hBCEC (G) cells; (C, H): merged images of A/B and F/G, respectively. (D, I): Complete blocking of NIR fluorescence of both U87MG cells (D) and HBCEC cells (I) demonstrating high $\alpha_v\beta_3$ integrin specificity of the conjugate. (E, J): direct visualization of U87MG (E) and HBCEC (J) cells under blocking condition.

Fig. 10A shows typical NIR fluorescence images of athymic nude mice bearing subcutaneous U87MG glioblastoma tumor after intravenous (i.v.) injection of 3 nmol of RGD-Cy5.5. The whole animal became fluorescent immediately after injection, and the subcutaneous U87MG tumor could be clearly delineated from the surrounding background tissue from 30 min to 24 h p.i. with maximum contrast occurring around 4 hr post-injection. Significantly amount of fluorescence was still detectable in the tumor at 48 h after contrast injection (data not shown). The fluorescence intensities defined as photons per second per centimeter squared per steradian (p/s/cm^2/sr) in the tumor and the normal tissues as a function of time are depicted in **Fig. 11**. The tumor uptake reached maximum at 2 h p.i. and slowly washed out over time. On the other hand, normal tissue had rapid uptake and relatively rapid clearance. The dose dependence of tumor-to-normal tissue contrast was also measured. Significant difference in tumor contrast was observed from 30 min to 4 h p.i. The mice injected with 3 nmol fluorescent probe had the lowest tumor contrast, while those with 0.5 nmol probe had the highest tumor contrast. The mice injected with 0.1 nmol probe had intermediate contrast. The difference diminished at 24 h time point. The tumor contrast was significantly higher at 60° than at 0° for both control and block animals.

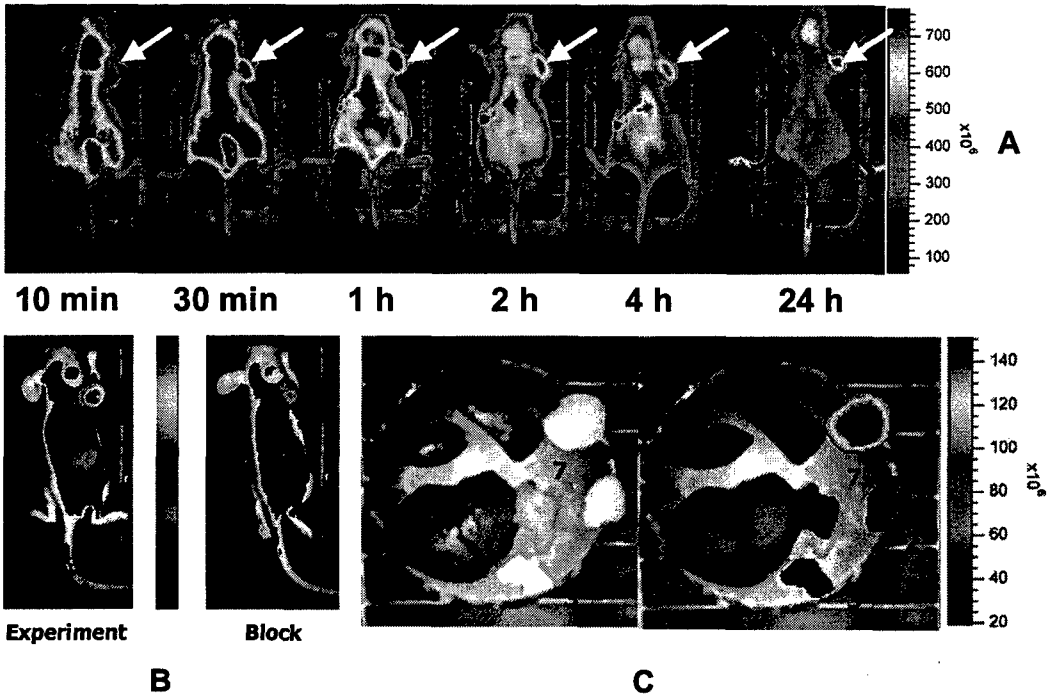

Fig. 10 (A) In vivo fluorescence imaging of subcutaneous U87MG glioblastoma tumor bearing athymic nude mice after intravenous injection of RGD-Cy5.5 conjugate. Dye labeled RGD peptide was administered at a dose of 3 nmol/mouse via a lateral tail vein. All NIR fluorescence images were acquired using a 120 s exposure time (f/stop = 4) and are normalized to the 10 min dorsal

image. The position of the tumor is indicated by an arrow. Fluorescence signal from Cy5.5 was pseudo-colored red. (B) Representative NIR images (60° mounting angle) of mice bearing subcutaneous U87MG tumor on the right shoulder demonstrating blocking of RGD-Cy5.5 (0.5 nmol) uptake in the tumors by co-injection with 10 mg/kg of c(RGDyK). Pseudo-color fluorescence images of tumor bearing mice were acquired 4 h after intravenous injection of RGD-Cy5.5 (left: experiment) or RGD-Cy5.5 + RGD (right: block). (C) Representative images of dissected organs of a mouse bearing U87MG tumor sacrificed 4 h after intravenous injection of RGD-Cy5.5 at a dose of 0.5 nmol equivalent Cy5.5/mouse. 1, U87MG tumor; 2, muscle; 3, pancreas; 4, liver; 5, kidney; 6, spleen; 7, lung.

In order to validate the specificity of the targeting process, we performed a blocking experiment. The control mice were each injected with 0.5 nmol of RGD-Cy5.5, and those as in the blocking experiment were each co-injected with 0.5 nmol of RGD-Cy5.5 and 10 mg/kg unlabeled RGD peptide (about 300 nmol). Tumor-to-normal tissue ratios at different viewing angles (0°, 45°, and 60°) were measured and typical NIR fluorescence images of U87MG tumor bearing mice mounted at 60° are shown in **Fig. 10B** (left: control; right: block). Unlabeled RGD peptide successfully reduced tumor contrast from 3.34 ± 0.38 to 1.43 ± 0.34. Furthermore, *ex vivo* evaluation of excised organs at 4 h post-injection (**Fig. 10C**) showed that the compound was predominantly taken up by the U87MG tumor, with both tumor fluorescence intensity and contrast significantly higher than those obtained from *in vivo* imaging ($P < 0.0001$).

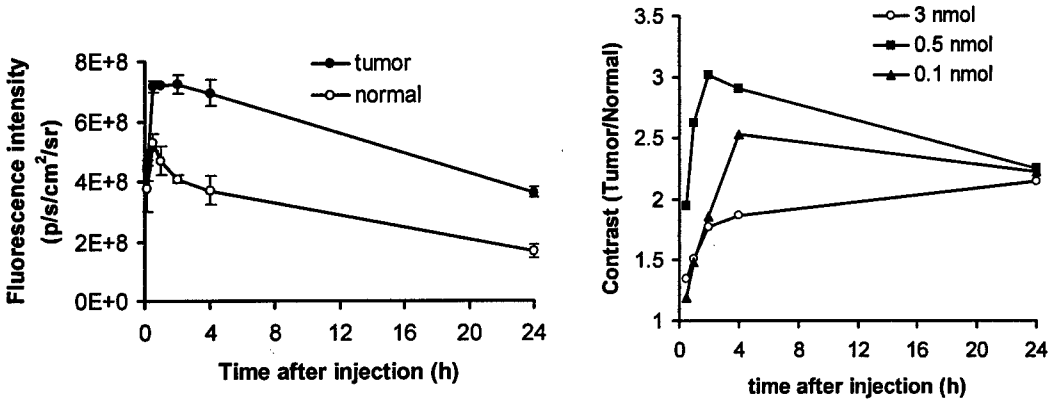

Fig. 11 (A): Quantification and kinetics of *in vivo* targeting character of RGD-Cy5.5 conjugate. Fluorescence intensity was recorded as photons per second per centimeter squared per steradian (p/s/cm^2/sr). Tumor fluorescence washout was slower than the normal tissue. (B) Dose dependent tumor contrast (tumor-to-normal tissue ratio) as a function of time postadministration: 3 nmol (○), 0.5 nmol (■), and 0.1 nmol (▲). The tumor contrast with intermediate dose (0.5 nmol) was significantly higher than both high dose (3 nmol) and low dose (0.1 nmol) at all time points examined.

We also tested the dimeric and tetrameric RGD peptides which had higher integrin binding affinity than the monomeric analog (**Fig. 12**) for NIR fluorescence imaging with Xenogen IVIS 200 system. The three conjugates were evaluated in a tumor xenograft model in order to investigate the effect of integrin avidity and molecular size of the RGD peptides on tumor targeting efficacy of the resulting Cy5.5 conjugates.

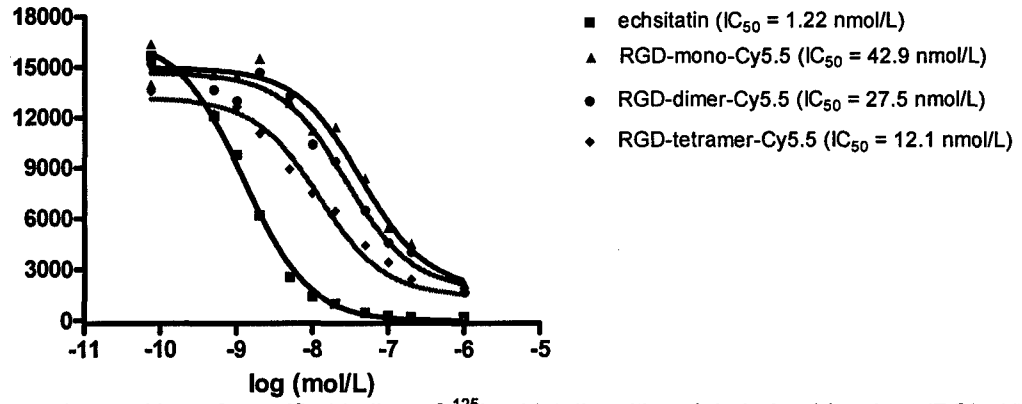

Fig. 12 Competition of specific binding of ^{125}I-echistatin with unlabeled echistatin, c(RGDyK)-Cy5.5, E[c(RGDyK)]$_2$-Cy5.5, and E[Ec(RGDyK)]$_2$]$_2$-Cy5.5 to integrin positive U87MG glioblastoma cells.

They all specifically accumulate in the integrin-expressing tumor cells in cell culture. The subcutaneous U87MG tumor can be clearly visualized with these three fluorescence probes. Moreover, the tumor uptake of the NIR probes can be inhibited by co-injection with c(RGDyK), demonstrating the in vivo integrin receptor targeting specificity of the Cydye-RGDs. The tumor/background ratios for Cy5.5-RGD tetramer are slightly higher than that of Cy5.5-RGD monomer and dimmer at all time points examined (**Fig. 13**).

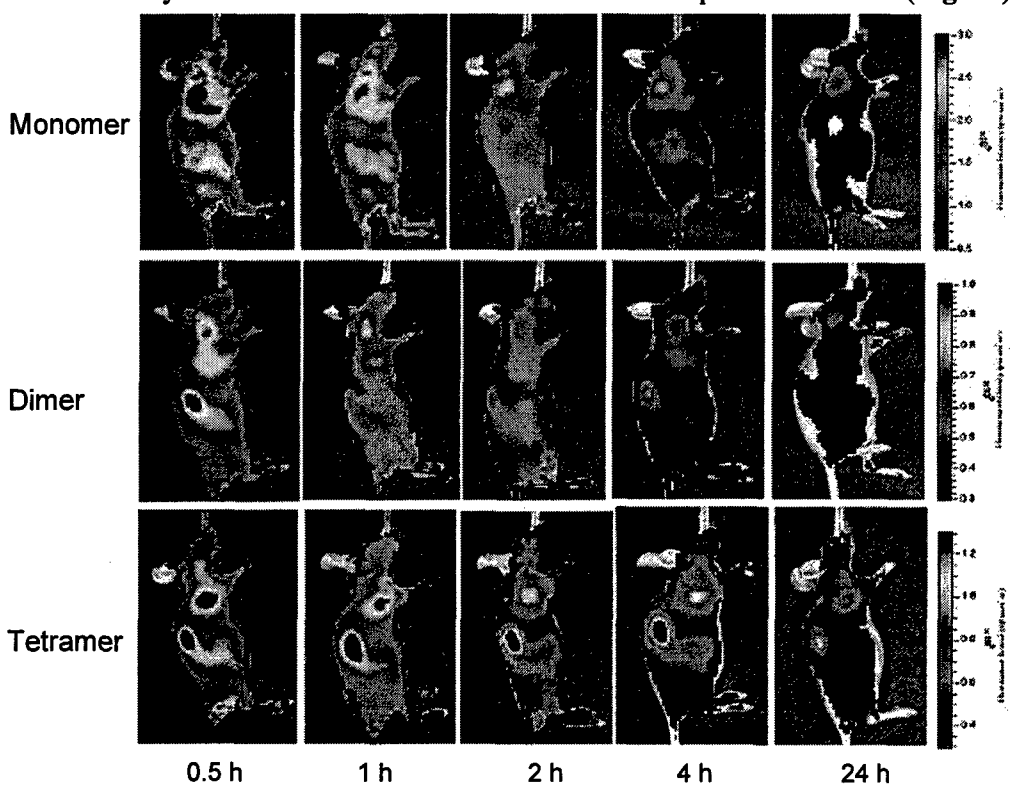

Fig. 13 Multiple time point near-infrared fluorescence imaging of subcutaneous U87MG glioblastoma tumor bearing athymic nude mice after intravenous injection of appropriate RGD-Cy5.5 conjugate. From top to bottom: c(RGDyK)-Cy5.5 (monomer), middle: E[c(RGDyK)]$_2$-Cy5.5 (dimer), bottom: E[E[c(RGDyK)]$_2$]$_2$-Cy5.5 (tetramer).

Encouraged by the ability of RGD-Cy5.5 conjugates to image subcutaneous U87MG glioma models, we applied both Cy5.5 labeled dimeric and tetrameric RGD peptides for androgen-independent breast cancer MDA-MB-435 tumor targeting. Cell binding assay using ^{125}I-echistatin as radioligand showed that both NIR probes had nanomolar binding affinity for integrin $\alpha_v\beta_3$ expressed on the surface of the tumor cells (**Fig. 14**). RGD tetramer provided long-lasting integrin specific uptake in the tumor and the tumor-to-background contrast was up to 3.5 (**Fig. 15**).

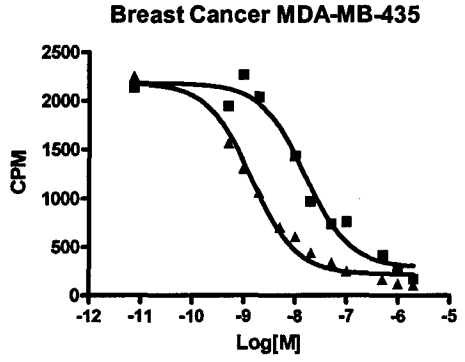

Fig. 14 Competition of specific binding of ^{125}I-echistatin with unlabeled echistatin, c(RGDyK)-Cy5.5, E[c(RGDyK)]$_2$-Cy5.5, and E[Ec(RGDyK)]$_2$]$_2$-Cy5.5 to integrin positive MDA-MB-435 breast cancer cells.

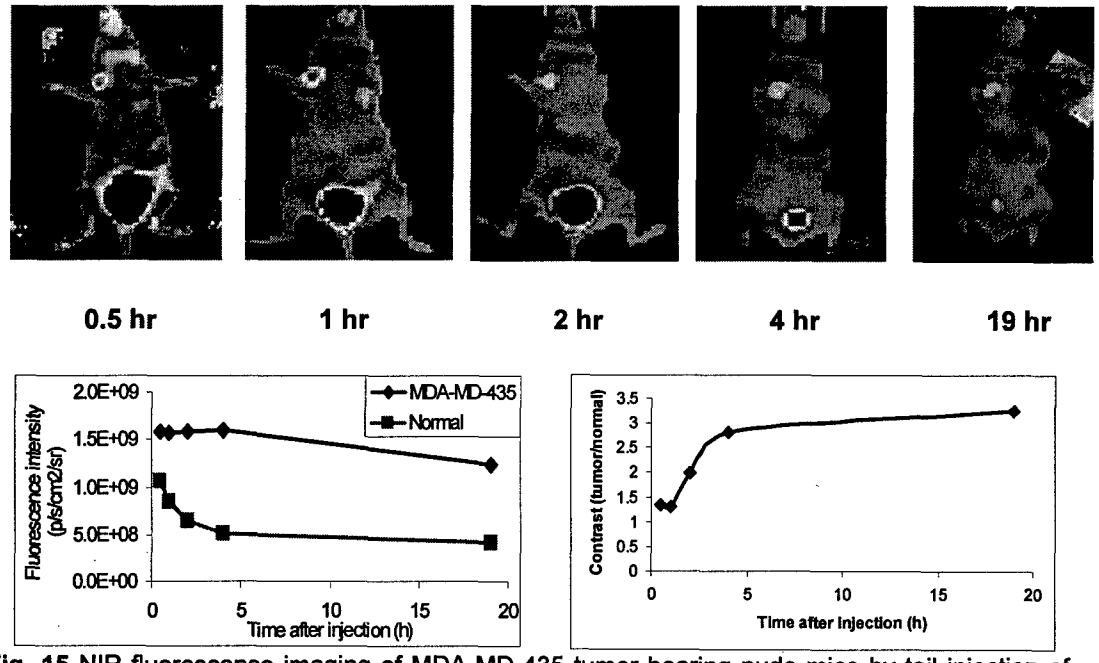

Fig. 15 NIR fluorescence imaging of MDA-MD-435 tumor bearing nude mice by tail injection of Cy5.5-E[E[c(RGDyK)$_2$]$_2$ (500 pmol/animal). The tumor activity accumulation reaches maxima at early times points and tumor contrast (as compared to contralateral background) increases with time elapsed.

KEY RESEARCH ACCOMPLISHMENTS

- Synthesized a series of cyclic RGD peptide antagonists of cell adhesion molecule integrin $\alpha_v\beta_3$;
- Conjugated RGD peptides with water-soluble quantum dots (EviTags);
- RGD-EviTag conjugates indicated receptor specific cell uptake and high photo-resistance, which turns out to be unstable in vivo;
- Fluorescent dye Cy5.5 labeled RGD peptides provides sensitive and semiquantitative NIR fluorescence imaging of integrin positive tumors including breast cancer.

REPORTABLE OUTCOMES

Publications partially supported by this grant:

1. Chen X, Conti PS, Moats RA. In vivo near-infrared fluorescence imaging of integrin alphavbeta3 in brain tumor xenografts. Cancer Res. 2004 Nov 1;64(21):8009-14.
2. Chen X, Hou Y, Tohme M, Park R, Khankaldyyan V, Gonzales-Gomez I, Bading JR, Laug WE, Conti PS. Pegylated Arg-Gly-Asp peptide: 64Cu labeling and PET imaging of brain tumor alphavbeta3-integrin expression. J Nucl Med. 2004 Oct;45(10):1776-83.
3. Chen X, Liu S, Hou Y, Tohme M, Park R, Bading JR, Conti PS. MicroPET imaging of breast cancer alphav-integrin expression with 64Cu-labeled dimeric RGD peptides. Mol Imaging Biol. 2004 Sep-Oct;6(5):350-9.
4. Chen X, Park R, Hou Y, Khankaldyyan V, Gonzales-Gomez I, Tohme M, Bading JR, Laug WE, Conti PS. MicroPET imaging of brain tumor angiogenesis with 18F-labeled PEGylated RGD peptide. Eur J Nucl Med Mol Imaging. 2004 Aug;31(8):1081-9.

Funding applied:

A R21 proposal in response to NCI RFA #: PAR-03-157, entitled: "Industry-Academic Partnership for Development of Biomedical Imaging System and Methods That Are Cancer Specific" was recently submitted. The proposal title is "Development of EviTag Quantum Dot for Tumor Angiogenesis Imaging".

CONCLUSIONS

Optical imaging, which uses neither ionizing radiation nor radioactive materials, is emerging as a complement to nuclear imaging methods. Near-infrared fluorescence emitting quantum dot nanoparticles and fluorescent dyes are both useful fluorophores for in vitro and in vivo applications. However, the surface coating of water-soluble quantum dots needs further systematic investigation to facilitate non-invasive in vivo imaging. RGD-Cy5.5 system provides the opportunity for rapid and cost-effective structure-activity studies to screen newly developed probes, before the more costly radionuclide-based imaging studies. A noninvasive imaging paradigm to image angiogenesis could provide a significant benefit to patient segmentation with cancer as well as with cardiovascular disease. Further development of more potent $\alpha_v\beta_3$ integrin antagonists for labeling Cy5.5 and other red-absorbing fluorescent dyes are now in progress for better tumor targeting and visualization of deep-lying tissues. The use of a time-domain optical imaging platform (*e.g.*, low-intensity pulsed laser source), instead of continuous wave technique (*e.g.*, tungsten light source), to obtain tomographic (three-dimensional) images and to subtract autofluorescence background based on their different fluorescence life time is also being explored.

REFERENCES

1. Bergers G, Benjamin LE (2003). Tumorigenesis and the angiogenic switch. *Nat Rev Cancer.* **3:**401-410.
2. Schirner M, Menrad A, Stephens A, Frenzel T, Hauff P, Licha K (2004). Molecular imaging of tumor angiogenesis. *Ann N Y Acad Sci.* **1014**:67-75.
3. Brooks PC, Clark RA, Cheresh DA (1994). Requirement of vascular integrin $\alpha_v\beta_3$ for angiogenesis. *Science.* **264**:569-5671.
4. Haubner R, Wester HJ (2004). Radiolabeled tracers for imaging of tumor angiogenesis and evaluation of anti-angiogenic therapies. *Curr Pharm Des.* **10**: 1439-1455.
5. Ntziachristos V, Bremer C, Weissleder R (2003). Fluorescence imaging with near-infrared light: new technological advances that enable in vivo molecular imaging. *Eur Radiol.* **13**:195-208.
6. Cheong WF, Prahl SA, Welch AJ (1990). A review of the optical properties of biological tissues. *IEEE J Quantum Electron.* **26**:2166-2185.
7. Jaiswal JK, Simon SM (2004). Potentials and pitfalls of fluorescent quantum dots for biological imaging. *Trends Cell Biol.* **14**:497-504.
8. Chen X, Conti PS, Moats RA (2004). In vivo near-infrared fluorescence imaging of integrin $\alpha_v\beta_3$ in brain tumor xenografts. *Cancer Res.* **64**:8009-8014.

APPENDICES

Reprints

Chen X, Conti PS, Moats RA (2004). In vivo near-infrared fluorescence imaging of integrin $\alpha_v\beta_3$ in brain tumor xenografts. *Cancer Res.* **64**:8009-8014.

[CANCER RESEARCH 64, 8009–8014, November 1, 2004]

In vivo Near-Infrared Fluorescence Imaging of Integrin $\alpha_v\beta_3$ in Brain Tumor Xenografts

Xiaoyuan Chen,[1,2] Peter S. Conti,[1] and Rex A. Moats[3]

[1]PET Imaging Science Center, University of Southern California Keck School of Medicine, Los Angeles, California; [2]Molecular Imaging Program at Stanford, Stanford University, Stanford, California; and [3]Departments of Pediatrics, Radiology, and Pathology, Children's Hospital Los Angeles, Los Angeles, California

ABSTRACT

Noninvasive visualization of cell adhesion molecule $\alpha_v\beta_3$ integrin expression *in vivo* has been well studied by using the radionuclide imaging modalities in various preclinical tumor models. A literature survey indicated no previous use of cyanine dyes as contrast agents for *in vivo* optical detection of tumor integrin. Herein, we report the integrin receptor specificity of novel peptide-dye conjugate arginine-glycine-aspartic acid (RGD)-Cy5.5 as a contrast agent *in vitro*, *in vivo*, and *ex vivo*. The RGD-Cy5.5 exhibited intermediate affinity for $\alpha_v\beta_3$ integrin (IC_{50} = 58.1 ± 5.6 nmol/L). The conjugate led to elevated cell-associated fluorescence on integrin-expressing tumor cells and endothelial cells and produced minimal cell fluorescence when coincubated with c(RGDyK). *In vivo* imaging with a prototype three-dimensional small-animal imaging system visualized subcutaneous U87MG glioblastoma xenograft with a broad range of concentrations of fluorescent probe administered via the tail vein. The intermediate dose (0.5 nmol) produces better tumor contrast than high dose (3 nmol) and low dose (0.1 nmol) during 30 minutes to 24 hours postinjection, because of partial self-inhibition of receptor-specific tumor uptake at high dose and the presence of significant amount of background fluorescence at low dose, respectively. The tumor contrast was also dependent on the mouse viewing angles. Tumor uptake of RGD-Cy5.5 was blocked by unlabeled c(RGDyK). This study suggests that the combination of the specificity of RGD peptide/integrin interaction with near-infrared fluorescence detection may be applied to noninvasive imaging of integrin expression and monitoring anti-integrin treatment efficacy providing near real-time measurements.

INTRODUCTION

Integrins $\alpha_v\beta_3$ and $\alpha_v\beta_5$ seem to play a critical role in regulating tumor growth and metastasis as well as tumor angiogenesis (1–5). Although only minimally expressed in quiescent blood vessels and normal cells, α_v integrins are significantly up-regulated in sprouting tumor vessels and solid tumor cells of various origins (4, 5), and their expression levels correlate well with the aggressiveness of the disease (6–8). Antibodies, small inhibitory peptides, and nonpeptide antagonists of α_v-integrins have thus been developed as potential antiangiogenic strategies (1, 9–11).

The ability to noninvasively visualize and quantify α_v-integrin level *in vivo* would allow us to understand the intrinsic relationship between α_v-integrin expression and tumor growth and spread, to evaluate anti-integrin treatment efficacy, and to develop new integrin antagonists of high potency (12, 13) with pertinent *in vivo* pharmacokinetics. With a similar aim in mind, researchers have labeled a series of monomeric and dimeric cyclic arginine-glycine-aspartic acid (RGD) peptides with different radionuclides for positron emission tomography (PET; refs. 14–17) and single-photon emission computed tomography (SPECT; 18, 19) imaging of α_v-integrin expression in various preclinical xenograft models, with tumor targeting efficacy and *in vivo* kinetics profiles being a factor of the receptor binding affinity and hydrophilicity, as well as of the metabolic stability of the radiotracers.

Although radionuclide imaging modalities are characteristic of high sensitivity and noninvasiveness, they often suffer from poor spatial and temporal resolution. Another characteristic of PET imaging, in particular, is the need for a local cyclotron to generate short-lived positron emitting radionuclides and a synthetic unit to produce the biologically useful probes. A relatively inexpensive, robust, and straightforward way of measuring integrin levels at least in a relative manner that also provides the possibility of semiquantitative evaluation would greatly aid the study of tumor biology. Optical imaging, which uses neither ionizing radiation nor radioactive materials, is emerging as a complement to nuclear imaging methods. The major limitation of light is the high absorption and scattering that occur in biological tissues and, thus, the limited penetration of the light through the body. However, in small animals, the required path-length of light is much shorter, which makes the use of optics more feasible. The ease of using short acquisition times also allows the collection of multiple time points and examinations in the same animal. Near-infrared (NIR) fluorescence imaging, in particular, is expected to have a major impact in biomedical imaging of specific targeting. In general, biological tissues exhibit a high photon absorbance in both the visible wavelength range (350–700 nm; secondary to hemoglobin, tissue pigments, and so forth) and in the infrared range (> 900 nm; secondary to lipids and water). However, in the NIR region (700–900 nm) the absorbance spectra for all biomolecules reach minima. Hence, NIR fluorescence light offers a unique advantage for the imaging of pathophysiological states (20). Thus, we chose the widely used Cy5.5 dye for our optical imaging studies.

NIR fluorescent dye Cy5.5 has proved to be a promising contrast agent for the *in vivo* demarcation of tumors by several groups (21–24). This dye has absorbance maximum at 675 nm and emission maximum at 694 nm, and can be detected *in vivo* at subnanomole quantities and at depths sufficient for experimental or clinical imaging depending on the NIR fluorescence image acquisition technique. In this study, we report *in vivo* NIR fluorescence imaging of integrin $\alpha_v\beta_3$-positive U87MG glioblastoma model targeted by a RGD-Cy5.5 conjugate. We demonstrate receptor specificity and long-lasting tumor accumulation of this fluorescent probe in human primary tumor cells in mouse xenografts.

MATERIALS AND METHODS

Materials. Cyclic RGD peptide [(c(RGDyK); M_r 617.6] was synthesized via solution cyclization of the fully protected linear pentapeptide H-Gly-Asp(OtBu)-D-Tyr(OtBu)-Lys[tert-butoxycarbonyl (Boc)]-Arg[2,2,4,6,7-pentamethyldihydrobenzofuran-5-sulfonyl (Pbf)]-OH, followed by trifluoroacetic acid deprotection (25). Cy5.5 monofunctional *N*-hydroxysuccinimide (NHS) ester (Cy5.5-NHS) and ^{125}I-labeled echistatin labeled by the lactoperoxidase method to a specific activity of 2,000 Ci/mmol were purchased from Amersham Biosciences (Piscataway, NJ). Echistatin was purchased from Sigma

Received 6/3/04; revised 8/23/04; accepted 8/27/04.

Grant support: Supported in part by National Institute of Biomedical Imaging and Bioengineering (NIBIB) grant R21 EB001785, Department of Defense (DOD) Breast Cancer Research Program (BCRP) Concept Award DAMD17-03-1-0752, DOD BCRP IDEA Award BC030012, American Cancer Society Institutional Research Grant ACS-IRG-580007-42, the Wright Foundation and Gunther Foundation, and National Cancer Institute P20 grant CA86532.

The costs of publication of this article were defrayed in part by the payment of page charges. This article must therefore be hereby marked *advertisement* in accordance with 18 U.S.C. Section 1734 solely to indicate this fact.

Requests for reprints: Xiaoyuan Chen, Molecular Imaging Program at Stanford, Stanford University, Stanford, CA 94305-5344. Phone: (650) 725-0950; Fax: (650) 736-0234; E-mail: shawchen@stanford.edu.

©2004 American Association for Cancer Research.

(St. Louis, MO). Chromalux HB microplates were obtained from Dynex Technologies (Chantilly, VA).

Synthesis and Characterization of RGD-Cy5.5. Cyclic RGD peptide [c(RGDyK; 3 mg, 4.84 μmol] dissolved in 1 mL of 0.1 mol/L sodium borate ($Na_2B_4O_7$) buffer (pH = 8.3) was mixed with Cy5.5-NHS (5.6 mg, 5 μmol) in H_2O (1 mL) in the dark at 4°C. After stirring overnight in the dark at 4°C, we quenched the reaction by adding 200 μL of 5% acetic acid (HOAc). The purification of the crude product was carried out on a semipreparative reversed-phase high-performance liquid chromatography (HPLC) system (Waters 515 chromatography system with a 486 tunable absorbance detector). Version 7.2.1 Labtech Notebook/XE software (Andover, MA) was used to record chromatograms. Purification was performed on a Vydac protein and peptide column 218TP510 (5 μm, 250 × 10 mm). The flow was 5 mL/minute, with the mobile phase starting from 95% solvent A (0.1% trifluoroacetic acid in water) and 5% solvent B (0.1% trifluoroacetic acid in acetonitrile; 0 to 2 minutes) to 35% solvent A and 65% solvent B at 32 minutes. The analytic HPLC method was performed with the same gradient system but with a Vydac 218TP54 column (5 μm, 250 × 4.6 mm) and flow was 1 mL/minute. The absorbance was monitored at 218 nm. The peak containing the RGD-Cy5.5 conjugate was collected, lyophilized, redissolved in saline at a concentration of 1 mg/mL, and stored in the dark at −80°C until use.

Solid-Phase Receptor Binding Assay. The standard assay was carried out as described previously with modifications (26). Microtiter-2 96-well plates were coated with 100 μL-per-well integrin $\alpha_v\beta_3$ (500 ng/mL) in coating buffer [25 mmol/L Tris–HCl (pH 7.4), 150 mmol/L NaCl, 1 mmol/L $CaCl_2$, 0.5 mmol/L $MgCl_2$, and 1 mmol/L $MnCl_2$] for 16 hours at 4°C, and the wells were blocked for 2 hours with 200 μL blocking buffer (coating buffer in the presence of 1% radioimmunoassay grade bovine serum albumin). The plate was washed twice with binding buffer (coating buffer in the presence of 0.1% bovine serum albumin) and then was incubated with ^{125}I-labeled echistatin (0.06 nmol/L) in the presence of different concentrations of RGD peptide (0.1 nmol/L to 5 μmol/L) at room temperature for 3 hours. After incubation, the plate was washed three times with binding buffer, and the radioactivity was solubilized with 2 mol/L boiling NaOH and was subjected to gamma-counting (Packard, Meriden, CT). Nonspecific binding of ^{125}I-labeled echistatin to $\alpha_v\beta_3$ was determined in the presence of 100 nmol/L echistatin. The IC_{50} values were calculated by nonlinear regression analysis with the GraphPad Prism computer-fitting program (GraphPad Software, Inc., San Diego, CA). Each data point is a result of the average of triplicate wells.

Cell Lines. Human glioblastoma cell line U87MG was obtained from American Type Culture Collection (Manassas, VA) and was maintained at 37°C in a humidified atmosphere containing 5% CO_2 in Iscove's modified Dulbecco's medium and 5% fetal bovine serum (Life Technologies, Inc., Grand island, NY). Primary human brain capillary endothelial cells (HBCECs) were isolated, characterized, and grown in RPMI 1640 with 10% fetal bovine serum in 5% CO_2 at 37°C.

Tumor Xenografts. Animal procedures were performed according to a protocol approved by the University of Southern California Institutional Animal Care and Use Committee. Female athymic nude mice (*nu/nu*), obtained from Harlan (Indianapolis, IN) at 4 to 6 weeks of age, were given injections subcutaneously in the right foreleg with 5×10^6 U87MG glioblastoma cells suspended in 100 μL of PBS. When the tumors reached 0.4 to 0.6 cm in diameter (14–21 days after implant), the tumor-bearing mice were subject to *in vivo* imaging studies.

Confocal Microscopy. We used a Leica TCS SP1 confocal optics, Ar ion (488 nm), Kr ion (568 nm), and HeNe (633 nm) lasers on a Leica DM IRBE microscope stand with HCX PL APO CS 63 ×/1.40 NA oil immersion objective lens, pinhole 1.0 Airy units, nominal Z resolution 236 nm, image (310 × 310-nm pixel size, medium speed, ~1 second per scan frame, 512 × 512 pixel image format, with 8 frame averaging. For laser confocal microscopy, cells grown on 35-mm MatTek imaging dishes (Cat no. P35G-0-14-C, Ashland, MA) were washed with PBS and then were incubated at 37°C in the presence of 100 nmol/L RGD-Cy5.5 for 1 hour. Afterward, cells were washed in ice-cold PBS and were examined with a TD488/568/633 dichroic beam splitter, simultaneous 488-nm excitation and photomultiplier tube-1 (PMT1) 522-to-578 nm emission for autofluorescence, 633-nm excitation, and PMT2 685-to-765 nm emission for RGD-Cy5.5 and both lasers for (nonconfocal) bright-field transmitted light. PMT1 and 2 were operated at high gain (1167 and 1054 V, respectively) and were offset adjusted such that the no-light noise floor was above gray value zero. There was no autofluorescence in PMT2 (Cy5.5 channel).

***In vivo* Optical Imaging System.** *In vivo* fluorescence imaging was performed with a prototype Xenogen IVIS three-dimensional small-animal *in vivo* imaging system (Xenogen, Alameda, CA), with both bioluminescence and fluorescence capabilities. The Xenogen instrument is a temperature-controlled, light-tight box with a cryogenically cooled back-illuminated digital charge-coupled device (CCD) camera, and anesthesia inlet and nose cone and gas outlet. For fluorescence a 150-W tungsten-halogen lamp is used with a light guide to a six-position excitation filter wheel. A second filter wheel, with large aperture to accommodate the camera, has six emission positions. Images and measurements of fluorescent signals were acquired and analyzed with Living Image software. An optimized Cy5.5 filter set was used for acquiring RGD-Cy5.5 fluorescence *in vivo*. Identical illumination settings (lamp voltage, filters) were used for all images, and fluorescence emission was normalized to photons per second per centimeter squared per steradian (p/s/cm^2/sr), as is common in bioluminescence imaging. Mice were given injections via tail vein with different amounts of RGD-Cy5.5 (0.1 to 3 nmol) and were anesthetized with 2 to 3% isoflurane (Abbott Laboratories) before they were placed in the Xenogen and imaged at various time points postinjection with a sampling of multiple angles while remaining sedated. A mouse that received an injection of 0.5 nmol of RGD-Cy5.5 was euthanized at 4 hours postinjection, the tumor and major tissue and organs were dissected, and fluorescence image was obtained.

Data Processing and Statistics. All of the data are given as means ± SD of n independent measurements. Statistical analysis was performed with a Student's t test. Statistical significance was assigned for P values < 0.05. For determining tumor contrast, mean fluorescence intensities and mean fluorescence intensities of the tumor (T) area at the right shoulder of the animal and of the corresponding area [normal tissue (N)] at the left shoulder were calculated by the region-of-interest function of Living Image software (Xenogen) integrated with Igor (Wavemetrics, Lake Oswego, OR). Dividing T by N yielded the contrast between tumor tissue and normal tissue.

RESULTS

Synthesis and Characterization of RGD-Cy5.5. The schematic molecule structure of c(RGDyK)-Cy5.5 conjugate (*RGD-Cy5.5*) is shown in Fig. 1. The NHS ester of the NIR fluorophore Cy5.5 is reacted with the ε-amino group of the lysine residue and purified by semipreparative HPLC. The absorption and fluorescence emission characteristics of RGD-Cy5.5 conjugate were similar to those of free Cy5.5, as apparent from the spectra measured in H_2O, except that the emission maximum slightly blue shifted from 694 nm (Cy5.5-NHS ester) to 690 nm (RGD-Cy5.5 conjugate). The yield of RGD-Cy5.5 conjugate was typically 70 to 75% as calculated with $\epsilon_{678\ nm} = 250{,}000\ (mol/L)^{-1}cm^{-1}$. The retention time on analytical HPLC was 16.6 minutes. Matrix-assisted laser desorption/ionization–time-of-flight mass spectrometry (MALDI-TOF MS): $m/z = 1518.4$ for $[M + H]^+$ (calculated M_r for $C_{68}H_{83}N_{11}O_{21}S_4$, 1518.7), $m/z = 1536.4$ for $[M + Na]^+$, and $m/z = 1556.4$ for $[M + K]^+$.

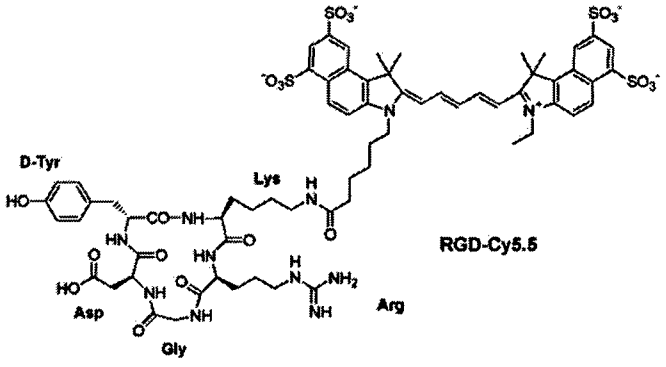

Fig. 1. Schematic structure of the RGD-Cy5.5 conjugate.

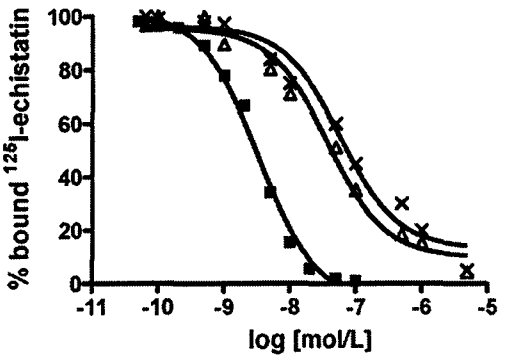

Fig. 2. Competition of specific binding of ^{125}I-labeled echistatin with unlabeled echistatin (■), c(RGDyK) (Δ), and c(RGDyK)-Cy5.5 (×) to purified $\alpha_v\beta_3$ integrin as determined with the solid-phase receptor assay. All of the points were done in triplicate. Cy5.5 conjugation did not significantly decrease the receptor binding affinity of the resulting fluorescent cyclic RGD peptide.

Receptor Binding Studies. To determine whether Cy5.5 conjugation had any effect on $\alpha_v\beta_3$ integrin receptor binding characteristics of the cyclic RGD peptide c(RGDyK), we measured the IC_{50} values of the RGD peptide analogues in competitive-type experiments. Binding of cold echistatin, c(RGDyK), and RGD-Cy5.5 competed with ^{125}I-labeled echistatin in a concentration-dependent manner (Fig. 2). Modification of the RGD peptide with Cy5.5 somewhat decreased its receptor binding avidity, with the IC_{50} values for c(RGDyK) and RGD-Cy5.5 being 37.5 ± 3.4 nmol/L and 58.1 ± 5.6 nmol/L, respectively.

To demonstrate that the RGD-Cy5.5 conjugate can act as a specific ligand for $\alpha_v\beta_3$ integrin receptor, the binding and subcellular localization of cyanine dye-labeled RGD peptide were incubated with U87MG tumor cells and HBCECs that are known to overexpress $\alpha_v\beta_3$ integrin. Negligible signals were detected in both cell lines when cells were incubated with Cy5.5 dye (data not shown). Receptor-mediated endocytosis of the RGD-Cy5.5 conjugate was observed by confocal laser-scanning microscopy in both cell types (Fig. 3*A, C* and *F, H*). Binding of RGD-Cy5.5 to both cell types was completely blocked by coincubation of the conjugate and c(RGDyK; 1 μmol/L; Fig. 3*D, I*).

***In vivo* Fluorescence Imaging with RGD-Cy5.5.** Figure 4*A* shows typical NIR fluorescence images of athymic nude mice bearing subcutaneous U87MG glioblastoma tumor after intravenous injection of 3 nmol of RGD-Cy5.5. The whole animal became fluorescent immediately after injection, and the subcutaneous U87MG tumor could be clearly delineated from the surrounding background tissue from 30 minutes to 24 hours postinjection with maximum contrast occurring ~4 hours postinjection. Significantly, the amount of fluorescence was still detectable in the tumor at 48 hours after contrast injection (data not shown). The fluorescence intensities defined as photons per second per centimeter squared per steradian (p/s/cm^2/sr) in the tumor and the normal tissues as a function of time are depicted in Fig. 5. The tumor uptake reached a maximum at 2 hours postinjection and slowly washed out over time. On the other hand, normal tissue had rapid uptake and relatively rapid clearance. The dose dependence of tumor-to-normal tissue contrast was also measured (Fig. 5). Substantial difference in tumor contrast was observed from 30 minutes to 4 hours postinjection The mice that were given injections of 3-nmol fluorescent probe had the lowest tumor contrast, whereas those with the 0.5-nmol probe had the highest tumor contrast. The mice injected with the 0.1-nmol probe had intermediate contrast. The difference diminished at the 24-hour time point. The tumor contrast was significantly higher at 60° than at 0° for both control and block animals.

To validate the specificity of the targeting process, we performed a blocking experiment. The control mice were each given injections of 0.5 nmol of RGD-Cy5.5, and those as in the blocking experiment were each given coinjections of 0.5 nmol of RGD-Cy5.5 and 10 mg/kg unlabeled RGD peptide (~300 nmol). Tumor-to-normal tissue ratios at different viewing angles (0°, 45°, and 60°) were measured (Table 1) and typical NIR fluorescence images of U87MG-tumor-bearing mice mounted at 60° are shown in Fig. 4*B* (*left*, control; *right*, block). Unlabeled RGD peptide successfully reduced tumor contrast from 3.34 ± 0.38 to 1.43 ± 0.34 (Table 1). Furthermore, *ex vivo* evaluation of excised organs at 4 hours postinjection (Fig. 4*C*) showed that the compound was predominantly taken up by the U87MG tumor, with both tumor fluorescence intensity and contrast significantly higher than those obtained from *in vivo* imaging ($P < 0.0001$).

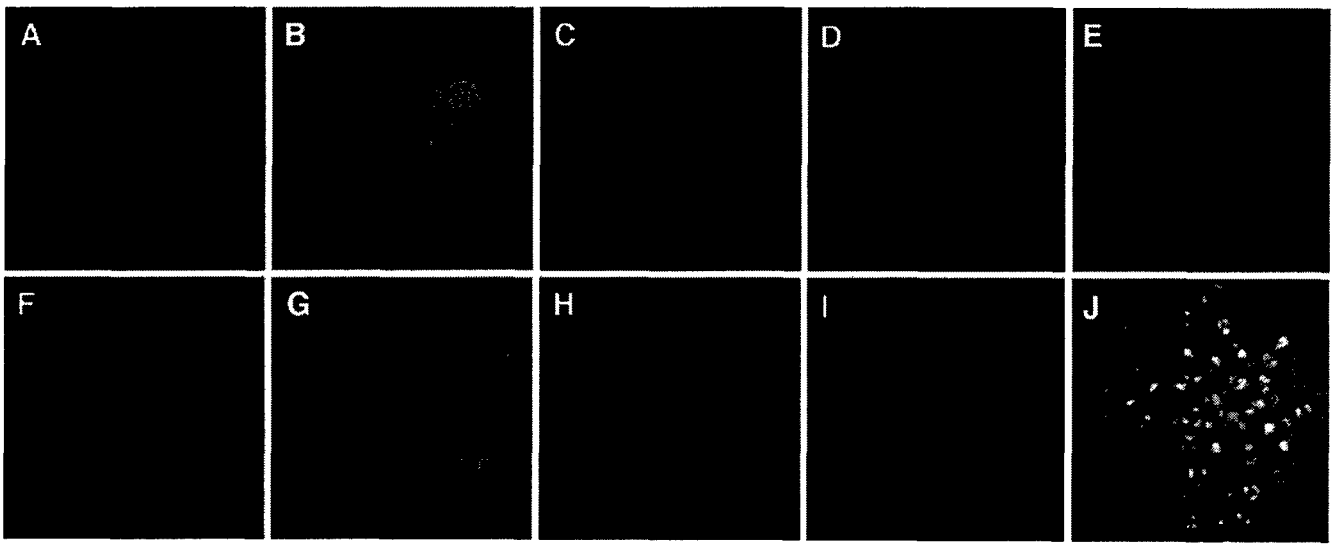

Fig. 3. Specific binding and endocytosis of the Cy5.5-labeled cyclic RGD peptide c(RGDyK). Confocal laser-scanning microscopy images of U87MG human glioblastoma (*A–E*) and HBCECs (*F–J*) incubated for 1 hour at 37°C in the presence of 100 nmol/L RGD-Cy5.5 with (*D–E, I–J*) or without (*A–C, F–H*) blocking dose of nonfluorescent RGD peptide c(RGDyK), 10 μmol/L. *A, F* NIR fluorescence images of U87MG (*A*) and HBCECs (*F*); *B, G*, direct visualization of U87MG (*B*) and HBCECs (*G*); *C, H*, merged images of *A/B* and *F/G*, respectively. *D, I*, complete blocking of NIR fluorescence of both U87MG cells (*D*) and HBCECs (*I*), demonstrating the high $\alpha_v\beta_3$ integrin specificity of the conjugate. *E, J*, direct visualization of U87MG (*E*) and HBCECs (*J*) under blocking condition.

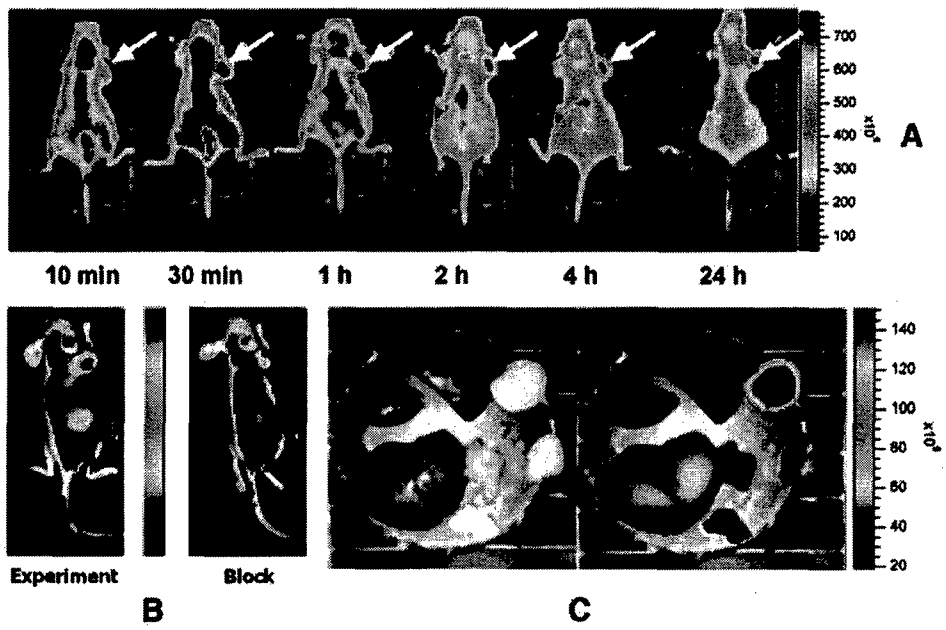

Fig. 4. *A, in vivo* fluorescence imaging of subcutaneous U87MG glioblastoma tumor-bearing athymic nude mice after intravenous injection of RGD-Cy5.5 conjugate. Dye-labeled RGD peptide was administered at a dose of 3 nmol/mouse via a lateral tail vein. All NIR fluorescence images were acquired with a 120-second exposure time (f/stop = 4) at 10 and 30 minutes (min) and at 1, 2, 4, and 24 hours (*h*) and are normalized to the 10-minute (*10 min*) dorsal image. *Arrow*, the position of the tumor. Fluorescence signal from Cy5.5 was pseudo-colored red. *B*, representative NIR images (60° mounting angle) of mice bearing subcutaneous U87MG tumor on the right shoulder demonstrating blocking of RGD-Cy5.5 (0.5 nmol) uptake in the tumors by coinjection with c(RGDyK), 10 mg/kg. Pseudo-color fluorescence images of tumor-bearing mice were acquired 4 hours after intravenous injection of RGD-Cy5.5 (*left, Experiment*) or RGD-Cy5.5 + RGD (*right, Block*). *C*, representative images of dissected organs of a mouse bearing U87MG tumor sacrificed 4 hours after intravenous injection of RGD-Cy5.5 at a dose of 0.5 nmol equivalent Cy5.5/mouse. *1*, U87MG tumor; *2*, muscle; *3*, pancreas; *4*, liver; *5*, kidney; *6*, spleen; *7*, lung.

DISCUSSION

The emergence of molecular imaging, as a result of unprecedented advances in molecular and cell biology and the availability of a cohort of molecular probes that are highly target specific, as well as the successful development of small-animal imaging instrumentation, allows noninvasive visualization of molecular events within living subjects. This emergence thus bridges the divide between the established findings from *in vitro* and cell culture assays and the clinical settings for disease interventions (27, 28). Molecular imaging has its root in nuclear medicine, which focuses on the management of patients through the use of injected radiotracers in conjunction with imaging technologies such as PET and SPECT (29). The underlying principle can now be tailored to other imaging modalities such as optical imaging (30).

Table 1 *Tumor-to-normal tissue ratios at 3 hours postinjection of control (0.5 nmol RGD-Cy5.5) and block (0.5 nmol RGD-Cy5.5 + 100 nmol RGD) mice at different mounting angles*

Mounting angle (°)	Control	Block
0	2.13 ± 0.28	0.85 ± 0.17
45	3.02 ± 0.45	1.33 ± 0.26
60	3.34 ± 0.38	1.43 ± 0.34

NOTE. The data are denoted as mean ± SD (n = 3).

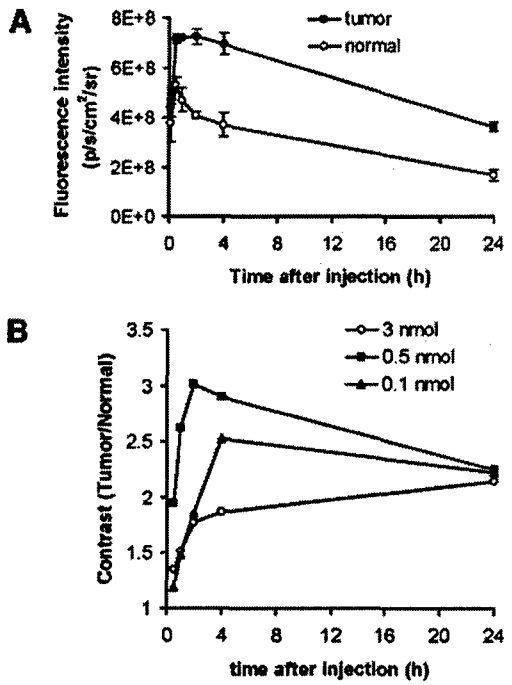

Fig. 5. *A*, quantification and kinetics of *in vivo* targeting character of RGD-Cy5.5 conjugate. Fluorescence intensity was recorded as photons per second per centimeter squared per steradian (*p/s/cm²/sr*). Tumor fluorescence washout was slower than that in the normal tissue. *B*, dose-dependent tumor contrast (tumor-to-normal tissue ratio) as a function of time[hour (*h*)] after administration: ○, 3 nmol; ■, 0.5 nmol; ▲, 0.1 nmol. The tumor contrast with intermediate dose (0.5 nmol) was significantly higher than for that with both high dose (3 nmol) and low dose (0.1 nmol) at all time points examined. [*E*, power (number, 10).]

Up-regulation of α_v integrins ($\alpha_v\beta_3$ and $\alpha_v\beta_5$) in tumor cells and tumor vasculature, relative to normal surrounding tissues, permits the preferential delivery of suitably labeled integrin antagonists to the receptor-positive tumors. Previous studies with radiolabeled cyclic RGD peptides demonstrated the site-specific localization of the tracers in the appropriate receptor-positive tumor cells and tumor vessels (14–19). Finding of these studies also showed a good correlation between the magnitude of tumor uptake and receptor expression levels. In our study, we described the selective retention of NIR dye Cy5.5-conjugated RGD peptide in tumors *in vivo*. Conjugation of Cy5.5 to RGD peptide did not have significant effect on the optical properties of Cy5.5 nor on the receptor binding affinity and specificity of the RGD peptide. Our optical imaging method now allows researchers to confirm the results of the radionucleotide studies with a complementary method.

Optical imaging strategies come from the recent development of targeted bioluminescence probes, fluorescent proteins, and exogenous fluorescent probes. The very sensitive, cryogenically cooled CCD camera allows for acquiring a fluorescence image superimposed on a gray-scale photographic image of the small animal with overlay and imaging analysis software. Although the Xenogen imaging system is sensitive enough to visualize the mice and delineate the tumor from background when as low as 0.1 nmol of dye-coupled RGD peptide was administered, the tumor contrast [fluorescence intensities of the

tumor (T) to those of normal tissue (N)] was significantly lower than that obtained by applying 0.5 nmol dye molecules ($P < 0.001$). The low T-to-N ratio at very "low dose" may be attributed to the interference of relatively high background fluorescence and Rayleigh and Raman scattering (31). It is not surprising that "high dose" (3 nmol) administration of fluorescent probe had the lowest tumor contrast at all of the time points examined. It is possible that partial self-inhibition of receptor-specific uptake in U87MG tumor had occurred during the imaging studies at such a high dose. The similar phenomenon was also observed in receptor-targeted radionuclide imaging (32). It is also noticeable that tumor fluorescence intensity and tumor contrast had significant difference at different mouse viewing angles. NIR fluorescence intensity is known to be a function of optical path-length between excitation light and target (33). The uneven character of the mouse and tumor surfaces as well as differences in skin thickness may also be responsible for different tumor contrast at different viewing angles.

Because of the limited tissue penetration ability of Cy5.5 dye, we are successful only in detecting the subcutaneous tumors; the same probe was unable to noninvasively visualize orthotopic U87MG glioblastoma implanted in the mouse forebrain although the dissected tissue indicated tumor-specific uptake of the fluorescent probe (data not shown). NIR fluorescence imaging probes that emit at longer wavelength, with considerably lower autofluorescence, lower tissue scattering, and more photon penetration into living tissue (34) may be desirable for intracranial lesion detection. Likewise, fluorescent impurities are significantly reduced with longer excitation and detection wavelength. Significantly less tumor contrast measured by noninvasive *in vivo* imaging (Fig. 4*A*) was observed than that directly measured by imaging the dissected tissues (Fig. 4*C*). Zaheer *et al.* (33) compared the osteoblastic activity; imaging with and without skin resulted in an intensity attenuation of 44%. This may be attributed to the loss of excitation and emission light density by penetrating the skin in addition to the scatter caused by the skin. It is expected that an NIR dye with longer excitation and emission wavelengths and an appropriate filter set will reduce the interference from the background and, thus, improve the tumor contrast and attain deeper penetration for visualization of deep-lying tumors and organs. The use of an optical coupling medium and/or tomographic imaging (35) may also be helpful to minimize the effects of skin scattering.

The receptor-mediated binding of Cy5.5-labeled RGD peptide to $\alpha_v\beta_3$ integrin was tested both *in vitro* and *in vivo*. Incubation of U87MG glioma cells and HBCECs in the presence of uncoupled Cy5.5 dye did not change the fluorescence signal of the cells (data not shown). However, RGD-Cy5.5 conjugate massively increased the fluorescence intensity of the cells, and the fluorescence was completely lost when the cells were incubated with a blocking dose of uncoupled RGD peptide (Fig. 2). The fluorescence signal was initially distributed over the cell surface and most likely associated with the plasma membrane, whereas prolonged incubation time resulted in endocytosis, with most of the fluorescence accumulated in the perinuclear region and disappeared almost completely from the membrane. The fluorescent dye conjugate also indicated integrin-specific tumor uptake, because the tumor contrast ablation was observed in a blocking experiment. It has been reported that some cyanine dyes are capable of tumor accumulation without conjugation with a specific targeting molecule (36), this may partially explain why the tumor contrast was not completely blocked by unconjugated RGD peptide (Fig. 4*B*). The residual contrast in the blocking experiment is probably due to accumulation in the extracellular space with some nonspecific binding. Simple blocking experiments demonstrate only that the uptake is tumor specific and saturable in a qualitative manner. Additional studies to correlate the magnitude of tumor uptake (signal brightness) with tumor receptor density distribution by immunohistochemistry and/or Western blotting are needed to validate the feasibility of noninvasive optical imaging to visualize α_v-integrin expression level *in vivo*.

Direct image of dissected tissues and organs revealed very good tumor-to-nontumor tissue ratios (Fig. 4*C*). The tumor-to-muscle ratio was almost twice as much as that observed from *in vivo* imaging at the same time point, simply because of more effective fluorescence detection without the interference from the skin. However, the quantification of *ex vivo* imaging of excised organs and tissues may not be a true reflection of tissue distribution of the RGD-Cy5.5 conjugate. The uptake in the liver and kidneys may be underestimated if the tracer was partially degraded and not detectable by the CCD camera because of the loss of fluorescence of the metabolites. Double labeling of RGD peptide with Cy5.5 and ^{125}I, and analyzing the biodistribution of this construct under the same conditions to correlate the fluorescence quantification and tissue activity accumulation of the conjugate, are required to confirm the *ex vivo* results.

In conclusion, our study successfully used the RGD peptide-$\alpha_v\beta_3$ integrin system to introduce a highly sensitive and semiquantitative NIR fluorescence imaging technique for tumor detection in preclinical animal models. To our knowledge, this is the first example of noninvasive imaging of integrin expression with optical modality. This approach provides the opportunity for rapid and cost-effective structure-activity studies to screen newly developed probes, before the more costly radionuclide-based imaging studies. A noninvasive imaging paradigm to image angiogenesis could provide a significant benefit to patient segmentation with cancer as well as with cardiovascular disease. Further development of more potent $\alpha_v\beta_3$ integrin antagonists for labeling Cy5.5 and other red-absorbing fluorescent dyes are now in progress for better tumor targeting and visualization of deep-lying tissues. The use of a time-domain optical imaging platform (*e.g.*, low-intensity pulsed laser source), instead of continuous wave technique (*e.g.*, tungsten light source), to obtain tomographic (three-dimensional) images and to subtract autofluorescence background based on their different fluorescence life time is also being explored.

ACKNOWLEDGMENTS

We thank Marvin D. Nelson, Jr., for use of the Xenogen system. The Leica confocal microscope is part of the Childrens Hospital Los Angeles (CHLA) Saban Research Institute's Congressman Julian Dixon Image Core. We thank the Image Core's George McNamara for operating the microscope, discussions, and manuscript review.

REFERENCES

1. Jin H, Varner J. Integrins: roles in cancer development and as treatment targets. Br J Cancer 2004;90:561–5.
2. Nisato RE, Tille JC, Jonczyk A, Goodman SL, Pepper MS. $\alpha_v\beta_3$ and $\alpha_v\beta_5$ integrin antagonists inhibit angiogenesis in vitro. Angiogenesis 2003;6:105–19.
3. Hodivala-Dilke KM, Reynolds AR, Reynolds LE. Integrins in angiogenesis: multitalented molecules in a balancing act. Cell Tissue Res 2003;314:131–44.
4. Cairns RA, Khokha R, Hill RP. Molecular mechanisms of tumor invasion and metastasis: an integrated view. Curr Mol Med 2003;3:659–71.
5. Felding-Habermann B. Integrin adhesion receptors in tumor metastasis. Clin Exp Metastasis 2003;20:203–213.
6. Gasparini G, Brooks PC, Biganzoli E, et al. Vascular integrin $\alpha_v\beta_3$: a new prognostic indicator in breast cancer. Clin Cancer Res 1998;4:2625–34.
7. Vonlaufen A, Wiedle G, Borisch B, Birrer S, Luder P, Imhof BA. Integrin $\alpha_v\beta_3$ expression in colon carcinoma correlates with survival. Mod Pathol 2001;14:1126–32.
8. Bello L, Francolini M, Marthyn P, et al. $\alpha_v\beta_3$ and $\alpha_v\beta_5$ integrin expression in glioma periphery. Neurosurgery 2001;49:380–9.
9. Shimaoka M, Springer TA. Therapeutic antagonists and conformational regulation of integrin function. Nat Rev Drug Discov 2003;2:703–16.
10. Hamm CW. Anti-integrin therapy. Annu Rev Med 2003;54:425–35.

11. Kumar CC. Integrin $\alpha_v\beta_3$ as a therapeutic target for blocking tumor-induced angiogenesis. Curr Drug Targets 2003;4:123–31.
12. McQuade P, Knight L. Radiopharmaceuticals for targeting the angiogenesis marker $\alpha_v\beta_3$. Q J Nucl Med 2003;47:209–20.
13. Haubner RH, Wester HJ, Weber WA, Schwaiger M. Radiotracer-based strategies to image angiogenesis. Q J Nucl Med 2003;47:189–99.
14. Chen X, Park R, Tohme M, Shahinian AH, Bading JR, Conti PS. MicroPET and autoradiographic imaging of breast cancer α_v-integrin expression using ^{18}F- and ^{64}Cu-labeled RGD peptide. Bioconjug Chem 2004;15:41–9.
15. Chen X, Park R, Shahinian AH, et al. ^{18}F-labeled RGD peptide: initial evaluation for imaging brain tumor angiogenesis. Nucl Med Biol 2004;31:179–89.
16. Haubner R, Kuhnast B, Mang C, et al. [^{18}F]Galacto-RGD: synthesis, radiolabeling, metabolic stability, and radiation dose estimates. Bioconjug Chem 2004;15:61–9.
17. Haubner R, Wester HJ, Weber WA, et al. Noninvasive imaging of $\alpha_v\beta_3$ integrin expression using ^{18}F-labeled RGD-containing glycopeptide and positron emission tomography. Cancer Res 2001;61:1781–5.
18. Janssen ML, Oyen WJ, Dijkgraaf I, et al. Tumor targeting with radiolabeled $\alpha_v\beta_3$ integrin binding peptides in a nude mouse model. Cancer Res 2002;62:6146–1.
19. Janssen M, Oyen WJ, Massuger LF, et al. Comparison of a monomeric and dimeric radiolabeled RGD-peptide for tumor targeting. Cancer Biother Radiopharm 2002;17: 641–6.
20. Becker A, Hessenius C, Licha K, et al. Receptor-targeted optical imaging of tumors with near-infrared fluorescent ligands. Nat Biotechnol 2001;19:327–33.
21. Ballou B, Fisher GW, Deng JS, Hakala TR, Srivastava M, Farkas DL. Cyanine fluorochrome-labeled antibodies in vivo: assessment of tumor imaging using Cy3, Cy5, Cy5.5, and Cy7. Cancer Detect Prev 1998;22:251–7.
22. Weissleder R, Tung CH, Mahmood U, Bogdanov A Jr. In vivo imaging of tumors with protease-activated near-infrared fluorescent probes. Nat Biotechnol 1999;17: 375–8.
23. Ke S, Wen X, Gurfinkel M, et al. Near-infrared optical imaging of epidermal growth factor receptor in breast cancer xenografts. Cancer Res 2003;63:7870–5.
24. Petrovsky A, Schellenberger E, Josephson L, Weissleder R, Bogdanov A Jr. Near-infrared fluorescent imaging of tumor apoptosis. Cancer Res 2003;63:1936–42.
25. Chen X, Park R, Shahinian AH, Bading JR, Conti PS. Pharmacokinetics and tumor retention of ^{125}I-labeled RGD peptide are improved by PEGylation. Nucl Med Biol 2004;31:11–19.
26. Kumar CC, Nie H, Rogers CP, et al. Biochemical characterization of the binding of echistatin to integrin $\alpha_v\beta_3$ receptor. J Pharmacol Exp Ther 1997;283:843–53.
27. Weissleder R, Mahmood U. Molecular imaging. Radiology 2001;219:316–33.
28. Massoud TF, Gambhir SS. Molecular imaging in living subjects: seeing fundamental biological processes in a new light. Genes Dev 2003;17:545–80.
29. Blasberg RG, Gelovani J. Molecular-genetic imaging: a nuclear medicine-based perspective. Mol Imaging 2002;1:280–300.
30. Choy G, Choyke P, Libutti SK. Current advances in molecular imaging: noninvasive in vivo bioluminescent and fluorescent optical imaging in cancer research. Mol Imaging 2003;2:303–12.
31. Buschmann V, Weston KD, Sauer M. Spectroscopic study and evaluation of red-absorbing fluorescent dyes. Bioconjug Chem 2003;14:195–204.
32. Chen X, Park R, Hou Y, et al. MicroPET and autoradiographic imaging of GRP receptor expression with ^{64}Cu-DOTA-[Lys^3]bombesin in human prostate adenocarcinoma xenografts. J Nucl Med 2004;45:1390–7.
33. Zaheer A, Lenkinski RE, Mahmood A, Jones AG, Cantley LC, Frangioni JV. In vivo near-infrared fluorescence imaging of osteoblastic activity. Nat Biotechnol 2001;19: 1148–54.
34. Quaresima V, Matcher SJ, Ferrari M. Identification and quantification of intrinsic optical contrast for near-infrared mammography. Photochem Photobiol 1998;67: 4–14.
35. Ntziachristos V, Bremer C, Graves EE, Ripoll J, Weissleder R. Fluorescence imaging with near-infrared light: new technological advances that enable in vivo molecular imaging. Eur Radiol 2003;13:195–208.
36. Licha K, Riefke B, Ntziachristos V, Becker A, Chance B, Semmler W. Hydrophilic cyanine dyes as contrast agents for near-infrared tumor imaging: synthesis, photophysical properties and spectroscopic in vivo characterization. Photochem Photobiol 2000;72:392–8.